Antiplane elastic wave propagation in pre-stressed periodic structures; tuning, band gap switching and invariance

CrossMark

Ellis G. Barnwell, William J. Parnell *, I. David Abrahams

School of Mathematics, University of Manchester, Manchester, M13 9PL, UK

HIGHLIGHTS

- Wave propagation in a pre-stressed periodic structure is considered.
- Band diagrams are found using the theory of small-on-large and it is shown that they are modified by pre-stress.
- It is found that stop bands can be switched on or off by application of a pre-stress.
- The choice of material has a significant effect on the stop band structure.
- By studying the notion of invariance, the concept of a phononic cloak is introduced.

ARTICLE INFO

ABSTRACT

The effect of nonlinear elastic pre-stress on antiplane elastic wave propagation in a two-dimensional periodic structure is investigated. The medium consists of cylindrical annuli embedded on a periodic square lattice in a uniform host material. An identical inhomogeneous deformation is imposed in each annulus and the theory of small-on-large is used to find the incremental wave equation governing subsequent small-amplitude antiplane waves. The plane-wave-expansion method is employed in order to determine the permissable eigenfrequencies. It is found that pre-stress significantly affects the band gap structure for Mooney–Rivlin and Fung type materials, allowing stop bands to be switched on and off. However, it is also shown that for a specific class of materials, their phononic properties remain invariant under nonlinear deformation, permitting some rather interesting behaviour and leading to the possibility of *phononic cloaks*.

© 2016 The Authors. Published by Elsevier B.V. This is an open access article under the CC BY license (http://creativecommons.org/licenses/by/4.0/).

1. Introduction

Complex materials are at the heart of modern-day engineering and technology. A vast number of such media possess an intricate microstructure that offers macroscopic behaviour that is not present in naturally occurring materials. In the field of acoustics and elastodynamics, phononic media and metamaterials present a wide array of opportunities for supporting and directing a multitude of wave types [1,2]. The ability to design these materials for a variety of wave filtering, focusing and directivity applications is greatly advantageous. In particular, it is desirable to create macroscopic properties that can be tuned in real time (so called *configurable* or *re-configurable* phononic media), rather than the medium having fixed dynamic properties from the outset. Predicting how the microstructure affects the macroscopic response on a static and dynamic level is pivotal to such design and control of these materials.

Employing inhomogeneous media in order to allow or restrict wave propagation has been discussed by numerous authors over the last century. The analysis of band gap formation in periodic elastic and acoustic media took off in earnest in the early 1990s, see e.g. [3–6] and the excellent recent review paper [7] for a broader literature review. Early work in tuning the acoustic response of such media focused on modifying band structures by rotating cylinders [8–10]. Others have utilised the tunability of a phononic crystal to create wave guides [11–13]. These latter works, however, generally rely on tuning the material at the design and construction phase, rather than allowing real-time tuning post-construction. This applies similarly to the work in photonics by e.g. Zhang et al. [14], which described how photonic band gaps could be enlarged by the use of a small volume fraction of a third material phase. In these situations, once manufactured, the medium has a fixed dynamic range.

As a method of performing external control over a crystal, several research groups have considered the influence of magnetic or electric fields [15,16]. In [17], an electric field is used to deform annular cylinders which are embedded in air. The use of piezoelectric materials has also been studied [18–20] and similarly, electro-rheological materials have recently been utilised [21]. Temperature control has been suggested as a mechanism for tuning [22,23] although typically the temperature effect on elastic properties is so small that control is only achievable through a phase transition. This mechanism provides the advantage of offering a phononic switch in such materials. Mechanical mechanisms to create *photonic* switches have also recently been considered, see e.g. [24,25].

The effect of a nonlinear pre-stress on elastic wave propagation has been studied previously in one dimension [26,27]. In [27] the stop and pass band structure was investigated and it was shown that the band structure can be manipulated effectively using pre-stress. Similar work was carried out in which an electric bias was studied as a mechanism for controlling the deformation in layered composites [28]. Another example in one dimension is the extension of an inhomogeneous beam [29], in which the manipulation and annihilation of stop bands is studied. An experimental investigation into one-dimensional structures was carried out in [30]. By making use of numerical simulations, via the finite-element method, the mechanical tunability of three-dimensional structures has also recently been studied [31]. Finally, the effect of microstructural buckling of an elastic material was the focus of investigation in [32,33].

The objective of this article is to introduce a new mechanism for tuning band gaps in the context of horizontally polarised shear (SH or antiplane) elastic waves, enabling the design of reversible phononic switches and configurable phononic media via a novel material geometry. The phononic medium studied is a two-dimensional periodic array of incompressible nonlinear elastic annular cylinders embedded in a homogeneous elastic host as depicted in Fig. 1. SH waves are polarised along the axes of the cylinders and propagate in the plane orthogonal to these axes. As shall be described in Section 2, the annular regions are pre-stressed whilst the host medium remains stress free. The influence of this pre-stress on linear wave propagation through the two-dimensional medium is then studied by first deriving the governing wave equation via application of the theory of small-on-large. In Section 3 the plane-wave-expansion (PWE) method is employed (in modified form) and extended in order to take into account the fact that the waves are propagating through a pre-stressed structure where the incremental moduli are strongly inhomogeneous. This method determines the associated dispersion curves very efficiently. In Section 4 the effect of the pre-stress on the structure is determined. Some concepts associated with phononic invariance are introduced including phononic equivalence and phononic cloaks. The possibility of phononic switching is then investigated for a variety of choices of strain energy function in the annulus phase. This new approach also permits the study of inhomogeneous deformation over and above changes in material geometry alone. Concluding remarks are offered in Section 5.

The restriction to the prescribed deformation, and to SH waves, is for clarity of exposition, focusing on the effect of the nonlinear pre-stress on wave propagation and the development of the new plane-wave-expansion technique. It also enables rather interesting results to be derived associated with invariance of phononic properties to pre-stress. More complex deformations and structures, as well as the full two-dimensional in-plane coupled compressional and shear wave problem will be described elsewhere.

2. Cylinder inflation and the incremental wave equation

In this section the geometry and properties of the medium are first described together with the initial deformation and the incremental wave equation governing superposed antiplane waves inside the material. As illustrated in Fig. 1 the medium consists of a two-dimensional square array (with period ℓ) of nonlinear elastic annular cylinders each with initial inner and outer radii R_0 and R_1 respectively, density ρ_1 and linear elastic shear moduli μ_1 embedded inside a homogeneous elastic host medium of density ρ_0 and linear elastic shear modulus μ_0. The unit cell is depicted in its stress-free state in Fig. 1(a). Each cylindrical annulus can in principal be pre-stressed independently but, in order to maintain periodicity, all are assumed to be subject to the same deformation. The latter consists of an inflation (leading to an inhomogeneous radial deformation) and extension along its axis such that, crucially here, the outer radius of the cylinder remains unchanged, $r_1 = R_1$. This results in a deformed configuration as depicted in Fig. 1(b). The host medium may be linear or nonlinear elastic. Since it is not subject to initial deformation this is irrelevant in the context of the problem studied here.

In order to determine the manner by which small amplitude waves propagate in the pre-stressed solid, the theory of small-on-large is employed. The majority of the technical details will be omitted here but can be found elsewhere, e.g. in [34,35]. In essence, the theory is based on a linearisation about the pre-stressed state, determining the equations that govern incremental waves in a body that has exhibited a finite static deformation.

It is assumed that the interior of each annular cylinder is filled with an inviscid gas such that no shear waves can propagate inside this cavity. This means that the SH waves are subject to traction-free conditions on the cavity boundary since no antiplane traction is imposed by the pre-stress. The precise deformation used in this paper was previously utilised for generating infinite [36] and finite [37] hyperelastic cloaks.

Although the deformation studied here may be considered as somewhat idealised, it exhibits similar features to other deformation states associated with more complex geometries. Furthermore, since the deformation can be defined in simple mathematical (analytical) form, the incremental moduli that arise in the governing wave equation can be written explicitly. This makes the modified application of the plane-wave-expansion method described in Section 3 more straightforward in this initial step. More complex lattice geometries could also be studied if one wished to incorporate additional tunable characteristics such as material anisotropy or multi-phase microstructure.

2.1. Initial deformation

The initial deformation of the annular region is the same as that used in [37,38]. The equations of nonlinear elasticity are considered with boundary conditions imposed on the inner and outer faces of the annulus and an imposed axial stretch. Body forces are neglected.

Using a cylindrical polar coordinate system with its origin at the centre of a cell, referred to as the fundamental periodic cell, consider an inflation of the cylindrical annulus due to an imposed pressure, p_0, acting on its inner surface, accompanied by an axial stretch ζ. The external face of the annulus is traction free. The deformation that ensues is written formally as

$$R = R(r), \qquad \Theta = \theta, \qquad Z = \frac{z}{\zeta}, \tag{1}$$

for some function $R(r)$ to be determined. The usual convention is followed, using upper (lower) case variables for the reference (deformed) configuration. The principal stretches in the directions r, θ and z respectively are given by

$$\lambda_r = \frac{1}{R'(r)}, \qquad \lambda_\theta = \frac{r}{R(r)}, \qquad \lambda_z = \zeta, \tag{2}$$

where the prime denotes differentiation with respect to the argument. The inner radius is permitted to change whilst the outer radius is fixed at R_1 by choosing ζ appropriately for the imposed pressure, i.e.

$$R_0 = R(r_0), \qquad R_1 = R(r_1) = r_1. \tag{3}$$

The second of (3) together with incompressibility ($\lambda_r \lambda_\theta \lambda_z = 1$) gives

$$R(r) = \sqrt{\zeta(r^2 + M)}, \tag{4}$$

where $M = (1/\zeta - 1)R_1^2$. One can either choose ζ and use (4) to find r_0, or choose r_0 and rearrange (4) to find ζ.

The radial Cauchy stress induced in the annular cylinders by the initial deformation can be determined by integrating the radial equation of equilibrium so that [39]

$$T_{rr}(r) = -p_0 + \int_{r_0}^{r} \frac{1}{s} \left(\lambda_\theta(s) \frac{\partial W}{\partial \lambda_\theta} - \lambda_r(s) \frac{\partial W}{\partial \lambda_r} \right) ds, \tag{5}$$

where W is the strain energy of the hyperelastic cylinder and $T_{rr}(r_0) = -p_0$ has been imposed on the inner surface. It is further stressed also that $T_{rr} = 0$ on $r = r_1$.

The aim now is to understand the influence that this deformation (within each annular cylinder) has on small-amplitude SH-wave propagation through the structure. It should be noted that the tractions required to apply the desired change in inner radius described above are taken to act only on the annular region and are maintained whilst the waves propagate. By ensuring that the outer radius remains fixed, no force is applied to the host phase and therefore it remains undeformed. One can consider a number of mechanisms to ensure that this deformation is possible in practice, including the consideration that the interface between the annulus and host allows sliding on a long timescale corresponding to the application of the finite deformation, whilst not permitting sliding on the short timescale associated with the small-amplitude linear elastic waves.

2.2. Incremental wave equation

Assume time-harmonic motion of the form $\exp(-i\omega t)$ where ω is the angular frequency of the wave. As with the initial deformation, the incremental wave equation in the periodic cell can be described effectively by using the polar coordinate system. However, when looking for global solutions, a slightly different approach is required as shall be seen shortly.

The theory of small-on-large can be employed to find the wave equation in the deformed annular region of the fundamental periodic cell. This theory is essentially a linearisation about deformed state, describing small-amplitude
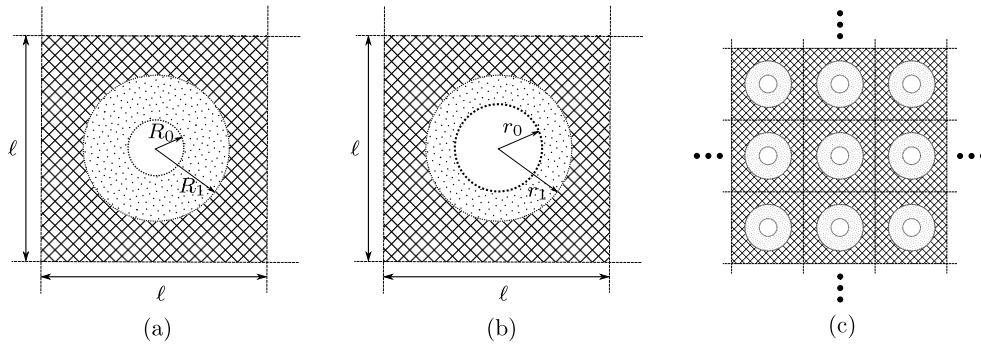
Fig. 1. Illustration of the unit cell for (a) the undeformed configuration and (b) the deformed configuration. The cylindrical annuli are embedded in a square periodic lattice with period ℓ in a stress-free, homogeneous medium shown by the hashed pattern. The periodic arrangement is illustrated in (c).

waves in the pre-stressed medium. The equation governing incremental antiplane waves polarised in the z direction, with displacements $w = w(r, \theta)$ is given by [36–38]

$$\frac{1}{r}\frac{\partial}{\partial r}\left(r\mu_r(r)\frac{\partial w}{\partial r}\right) + \frac{1}{r^2}\frac{\partial}{\partial \theta}\left(\mu_\theta(r)\frac{\partial w}{\partial \theta}\right) + \rho\,\omega^2 w = 0, \tag{6}$$

where $\rho = \rho_1$ is the constant mass density in the annulus $r_0 < r < r_1$. Note that since the material is incompressible the density of the annulus is unaffected by the pre-stress. As the limit of no deformation is approached, the equation above reduces to the usual linear wave equation.

The incremental shear moduli $\mu_r(r)$ and $\mu_\theta(r)$ are dependent on the specific form of strain energy function, $W(\lambda_r, \lambda_\theta, \lambda_z)$, that is used to model the nonlinear elastic response of the annular cylinders, and their general forms can be written down as [35,38]

$$\mu_r(r) = \left(\frac{\lambda_r\frac{\partial W}{\partial \lambda_r} - \lambda_z\frac{\partial W}{\partial \lambda_z}}{\lambda_r^2 - \lambda_z^2}\right)\lambda_r^2, \qquad \mu_\theta(r) = \left(\frac{\lambda_\theta\frac{\partial W}{\partial \lambda_\theta} - \lambda_z\frac{\partial W}{\partial \lambda_z}}{\lambda_\theta^2 - \lambda_z^2}\right)\lambda_\theta^2. \tag{7}$$

Note that the shear moduli in the pre-stressed annular cylinders are inhomogeneous and exhibit cylindrical anisotropy due to the imposed deformation and induced stress fields. When there is no pre-stress $\mu_r = \mu_\theta = \mu_1$. Because the host medium remains stress free, the shear moduli in this region are isotropic and homogeneous. The governing wave equation in the host, $r > r_1$, is then given by (6) with $\mu_r = \mu_\theta = \mu_0$ and $\rho = \rho_0$. The region inside the annular cylinder is occupied by an inviscid fluid at constant pressure and hence no shear waves can propagate in this region.

As described above, the incremental equation (6) applies on the fundamental periodic cell, i.e. to each annular cylinder with its centre as the origin of a local cylindrical polar coordinate system. However, solving this equation globally for the wave and imposing appropriate periodicity conditions with respect to polar coordinates would be rather awkward, if not impossible. So, planar Cartesian coordinates x, y are introduced related to the polar coordinates in the usual manner, $x = r\cos\theta, y = r\sin\theta$ and the notation $\mathbf{x} = (x, y)$ is employed: the medium is periodic with respect to $\mathbf{x}$. It is therefore useful to re-write the incremental equation on the unit cell with respect to these Cartesian coordinates when the plane-wave-expansion method is introduced in Section 3. Before this, explicit forms for the incremental moduli are derived for two popular strain energy functions for nonlinear materials.

2.3. Strain energy functions

2.3.1. The Mooney–Rivlin strain energy function

For an incompressible Mooney–Rivlin material, the strain energy function is given by

$$W = \frac{\mu}{2}\left(S_1(\lambda_r^2 + \lambda_\theta^2 + \lambda_z^2 - 3) + (1 - S_1)(\lambda_r^2\lambda_\theta^2 + \lambda_r^2\lambda_z^2 + \lambda_\theta^2\lambda_z^2 - 3)\right), \tag{8}$$

where $S_1 \in [0, 1]$ is an empirically determined material constant. A neo-Hookean material corresponds to taking $S_1 = 1$. The Mooney–Rivlin model is typically used to describe rubber-like materials and is said to be more realistic than the neo-Hookean model at large deformations.

It has been shown that for a Mooney–Rivlin material, the shear moduli in the annular region, $\mu_r(r)$ and $\mu_\theta(r)$, are given by [39]

$$\mu_j(r) = \frac{T\mu_1}{\zeta^2}\left(1 + \frac{m}{f_j(r)}\right) \quad \text{for } r_0 < r < r_1, \tag{9}$$

with $j = r, \theta$ where $f_r(r) = r^2, f_\theta(r) = -(r^2 + M)$ and the parameters m and T are defined as $T = 1 + (\zeta - 1)S_1, m = M\zeta S_1/T$.

In the case of a neo-Hookean solid ($S_1 = 1$) with specific material properties, a perfect (in principal) finite cloak can be theoretically observed using the deformation described in Section 2.1, provided $\mu_1 = \zeta \mu_0$ and $\rho_1 = \zeta \rho_0$ [37]. This implies that the scattering behaviour in the deformed state is identical to the stress-free case. The notion is employed to give rise to two effects in Sections 4.1 and 4.2 associated with the invariance of the phononic response to pre-stress.

2.3.2. The Fung strain energy function

Since the Mooney–Rivlin strain energy function is essentially an extension of the Neo-Hookean, an alternative strain energy function is studied in order to assess its influence on the tunability of band gaps. The chosen form is a simplified version of the Fung strain energy function given by [40]

$$W = \frac{\mu_1}{2} \left(e^Q - 1 \right), \tag{10}$$

where $Q = \frac{1}{2} \left(\lambda_r^2 + \lambda_\theta^2 + \lambda_z^2 - 3 \right)$. This strain energy function is often used to model soft biological tissues.

The incremental shear moduli in the annular region for this case are

$$\mu_j(r) = \frac{\mu_1 \alpha_j (r^2 + M)}{2r^2} \left(\frac{\alpha_j (r^2 + M)}{r^2} + \zeta - 1 \right) e^Q, \tag{11}$$

with $j = r, \theta$, where $\alpha_r = 1/\zeta$, $\alpha_\theta = \zeta$. As shall be seen, significant differences in incremental moduli arise due to the choice of strain energy function, a detail that manifests itself in a strongly modified material response to incremental waves.

3. Plane-wave-expansion (PWE) method

The plane-wave-expansion method has been found to be a highly efficient technique to derive the band gap structure of periodic media [5]. In general however this method is applied to materials where each phase is homogeneous and therefore the coefficients appearing in the governing equations are usually simply piecewise-constant. Here the method is adapted to the case where material properties are permitted to be inhomogeneous *within phases*. Furthermore, it is noted that although polar coordinates are a natural representation for the geometry of the cylindrical annuli and imposition of boundary conditions, the PWE naturally accounts for any jumps in material properties and therefore what is important is to impose periodicity, which in this case is in the x and y directions. As such transformation of the incremental equation to Cartesian coordinates is necessary.

The PWE scheme represents the displacement as a sum of plane waves modulated by a Bloch phase term in order to ensure quasi-periodicity of the propagating wave. In doing this, a matrix eigenvalue problem is obtained for the permitted frequencies of a given Bloch wavenumber. In the present case, the displacement $w(\mathbf{x})$ in (6) is written as

$$w(\mathbf{x}) = e^{i\mathbf{K} \cdot \mathbf{x}} \sum_{\mathbf{G}} W[\mathbf{G}] e^{i\mathbf{G} \cdot \mathbf{x}}, \tag{12}$$

where $\mathbf{K}$ is the Bloch wavevector, $\mathbf{G}$ are the reciprocal lattice vectors and $W[\mathbf{G}]$ are the Fourier coefficients of the displacement. The sum in (12) is over all possible reciprocal lattice vectors, which for a square lattice of period ℓ, are given by

$$\mathbf{G} = \frac{2\pi}{\ell} \left(m\mathbf{e}_x + n\mathbf{e}_y \right), \tag{13}$$

where $\mathbf{e}_x$ and $\mathbf{e}_y$ are unit vectors in the x and y directions and m and n span the integers. The sum in Eq. (12) is a double sum over both m and n.

Since periodicity is with respect to Cartesian coordinates, in order to proceed with the implementation of the PWE, Eq. (6) must be transformed. Note that (6) can be written in the form

$$\nabla \cdot (\mathbf{e}_r \sigma_{zr} + \mathbf{e}_\theta \sigma_{z\theta}) + \rho \omega^2 w = 0 \tag{14}$$

where $\mathbf{e}_r$ and $\mathbf{e}_\theta$ are unit vectors in the radial and azimuthal directions, $\sigma_{zr} = \mu_r \partial w / \partial r$ and $\sigma_{z\theta} = \mu_\theta / r \partial w / \partial \theta$. It is straightforward to show that this becomes, in Cartesian coordinates,

$$\nabla \cdot (\mathbf{e}_x \sigma_{zx} + \mathbf{e}_y \sigma_{zy}) + \rho \omega^2 w = 0 \tag{15}$$

where $\sigma_{zx} = C_{zxzx} \partial w / \partial x + C_{zxzy} \partial w / \partial y$, $\sigma_{zy} = C_{zyzx} \partial w / \partial x + C_{zyzy} \partial w / \partial y$ and

$$C_{zxzx} = \frac{1}{x^2 + y^2} (x^2 \mu_r + y^2 \mu_\theta), \tag{16}$$

$$C_{zxzy} = C_{zyzx} = \frac{xy}{x^2 + y^2} (\mu_r - \mu_\theta), \tag{17}$$

$$C_{zyzy} = \frac{1}{x^2 + y^2} (y^2 \mu_r + x^2 \mu_\theta). \tag{18}$$

These can now be written in the form of Fourier series:

$$C_{zxzx}(\mathbf{x}) = \sum_{\mathbf{G}} \mu_{xx}[\mathbf{G}]e^{i\mathbf{G}\cdot\mathbf{x}}, \qquad \mu_{xx}[\mathbf{G}] = \frac{1}{A}\int_{Cell} C_{zxzx}(\mathbf{x})e^{-i\mathbf{G}\cdot\mathbf{x}}d\mathbf{x}, \tag{19}$$

$$C_{zxzy}(\mathbf{x}) = \sum_{\mathbf{G}} \mu_{xy}[\mathbf{G}]e^{i\mathbf{G}\cdot\mathbf{x}}, \qquad \mu_{xy}[\mathbf{G}] = \frac{1}{A}\int_{Cell} C_{zxzy}(\mathbf{x})e^{-i\mathbf{G}\cdot\mathbf{x}}d\mathbf{x}, \tag{20}$$

$$C_{zyzy}(\mathbf{x}) = \sum_{\mathbf{G}} \mu_{yy}[\mathbf{G}]e^{i\mathbf{G}\cdot\mathbf{x}}, \qquad \mu_{yy}[\mathbf{G}] = \frac{1}{A}\int_{Cell} C_{zyzy}(\mathbf{x})e^{-i\mathbf{G}\cdot\mathbf{x}}d\mathbf{x} \tag{21}$$

where $A = \ell^2$ is the area of the periodic cell. Employing these in (15) it is easily shown that

$$\sum_{\mathbf{G}'}\Bigg[\sum_{\mathbf{G}} \mu_{xx}[\mathbf{G}' - \mathbf{G}](K_x + G_x')(K_x + G_x) + \mu_{xy}[\mathbf{G}' - \mathbf{G}]((K_x + G_x')(K_y + G_y) + (K_y + G_y')(K_x + G_x))$$

$$+ \mu_{yy}[\mathbf{G}' - \mathbf{G}](K_y + G_y')(K_y + G_y) - \omega^2 \mathcal{R}[\mathbf{G}' - \mathbf{G}]\Bigg]W[\mathbf{G}]e^{i(\mathbf{K}+\mathbf{G}')\cdot\mathbf{x}} = 0 \tag{22}$$

noting that $\mathbf{K} = K_x\mathbf{e}_x + K_y\mathbf{e}_y$, $\mathbf{G} = G_x\mathbf{e}_x + G_y\mathbf{e}_y$ and ρ has also been written in Fourier series form with Fourier coefficients $\mathcal{R}[\mathbf{G}]$. The exponential term is separated from the sum over $\mathbf{G}$. Since this equation must be true for any $\mathbf{x}$, it must be the case that for every $\mathbf{G}'$ the sum over $\mathbf{G}$ must be zero, i.e.

$$\Bigg[\sum_{\mathbf{G}} \mu_{xx}[\mathbf{G}' - \mathbf{G}](K_x + G_x')(K_x + G_x) + \mu_{xy}[\mathbf{G}' - \mathbf{G}]((K_x + G_x')(K_y + G_y) + (K_y + G_y')(K_x + G_x))$$

$$+ \mu_{yy}[\mathbf{G}' - \mathbf{G}](K_y + G_y')(K_y + G_y) - \omega^2 \mathcal{R}[\mathbf{G}' - \mathbf{G}]\Bigg]W[\mathbf{G}] = 0. \tag{23}$$

This is now seen to be in the form of a generalised eigenvalue problem and will give the full dispersion relation associated with the medium. It is conventional to scan around the outside of the irreducible Brillouin zone and pick out the lowest frequency modes [6,41].

4. Results

When presenting results associated with dispersion relations, the band diagrams will be plotted in the usual manner. That is, the frequency of each mode is determined whilst scanning the wavenumber around the edge of the irreducible Brillouin zone, as described in [2]. Following convention, the three points defining this boundary are denoted Γ ($\hat{\mathbf{K}} = 0\mathbf{i} + 0\mathbf{j}$), X ($\hat{\mathbf{K}} = 0.5\mathbf{i} + 0\mathbf{j}$) and M ($\hat{\mathbf{K}} = 0.5\mathbf{i} + 0.5\mathbf{j}$).

Throughout the results section, the shear modulus and density are non-dimensionalised on those of the host material and the wavenumbers on the lattice period ℓ, i.e.

$$\hat{\mu}(\mathbf{x}) = \frac{\mu(\mathbf{x})}{\mu_0}, \qquad \hat{\rho}(\mathbf{x}) = \frac{\rho(\mathbf{x})}{\rho_0}, \qquad \hat{\mathbf{K}} = \ell\mathbf{K}, \qquad \hat{\mathbf{G}} = \ell\mathbf{G}. \tag{24}$$

The nondimensional frequency therefore becomes

$$\hat{\omega} = \frac{\ell\omega}{c_0}, \tag{25}$$

where $c_0 = \sqrt{\mu_0/\rho_0}$ is the shear wave speed in the host material (and unstressed annulus due to the choice of properties above). Through non-dimensionalising the spatial variable on the period, ℓ,

$$\hat{x} = \frac{x}{\ell}, \qquad \hat{y} = \frac{y}{\ell} \tag{26}$$

the unit cell is mapped to the region $-1/2 < \hat{x} < 1/2$ and $-1/2 < \hat{y} < 1/2$. The outer radius of the pre-stressed region remains fixed at $R_1 = r_1 = 0.45$. This value was chosen since it is large enough to give a sizeable pre-stressed region, but not too large so the pre-stressed region is close to the outer edge of the unit cell. Although it is possible to study the latter case as r_1 gets closer to 0.5, a significant increase in the number of terms in the PWE is required. Since this is not the main focus of the study it is avoided here.

For all calculations, the maximum plane wave number is taken at 10 (corresponding to 441 plane waves) which has been established to give sufficiently accurate results. The percentage error in the method is estimated by taking a large number of plane waves and is typically below 0.05%.

The determination of analytical results and equivalence properties associated with the neo-Hookean medium in particular allows two interesting observations to be made before the notion of configurable band gaps are considered.
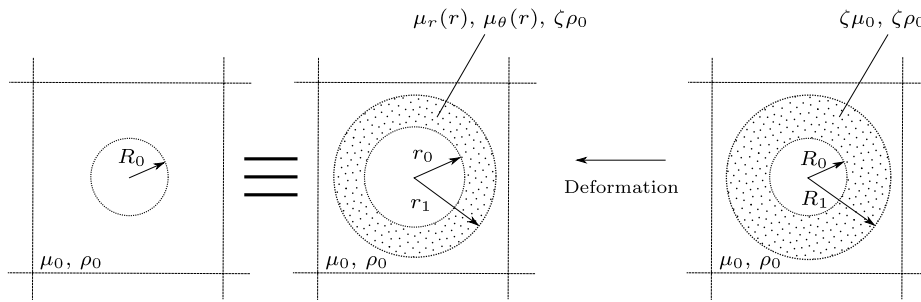
Fig. 2. Illustration of phononic equivalence. The medium on the left, consisting of a periodic array of cavities in a homogeneous medium with shear modulus μ_0 and density ρ_0 has a specific band gap structure. The medium in the middle, consisting of a periodic array of cylindrical annuli with shear modulus μ_1 and density ρ_1 embedded in a homogeneous medium with shear modulus μ_0 and density ρ_0, is phononically equivalent to the medium on the left when the annuli are pre-stressed with axial stretch ζ if $\mu_1 = \zeta\mu_0$, $\rho_1 = \zeta\rho_0$. The equivalent material in its undeformed state is shown on the far right.
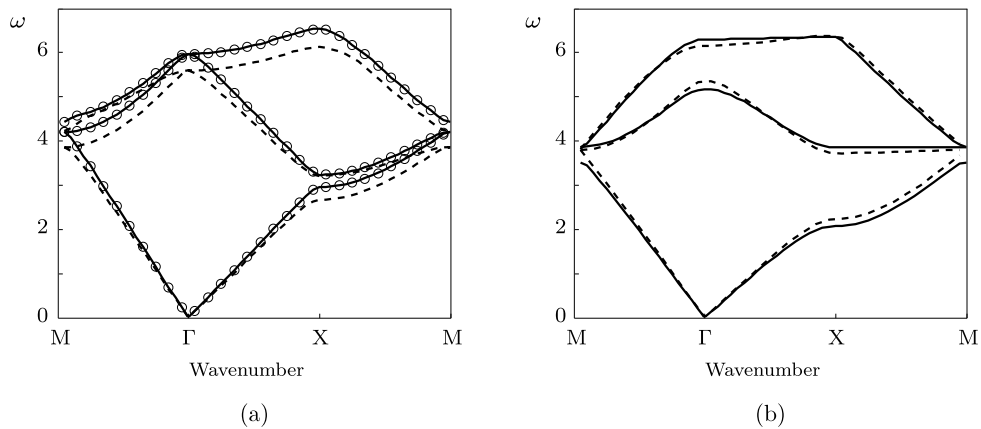

Fig. 3. (a) Dispersion curves associated with a stress-free medium (solid lines) with a square periodic array of cylindrical cavities of radius $R_0 = 0.1$. Overlaid circles are results associated with a square array of pre-stressed neo-Hookean cylindrical annuli, with $R_0 = 0.1$, $\zeta = 1.4$ and $r_0 = 0.255$ with shear modulus $\mu_1 = \zeta\mu_0$ and density $\rho_1 = \zeta\rho_0$. The dashed line corresponds to the response in the same pre-stressed state but when the annuli are of Mooney–Rivlin type with $S_1 = 0.6$. (b) Dispersion curves associated with a stress-free medium (solid lines) with a square periodic array of cylindrical cavities of radius $R_0 = 0.35$ with a band gap evident. These are compared with dispersion curves associated with a square array of pre-stressed neo-Hookean cylindrical annuli, with $R_0 = 0.3$, $\zeta = 1.4$ and $r_0 = 0.35$ (i.e. pre-stressed to the same geometry) with shear modulus $\mu_1 = \zeta\mu_0$ and density $\rho_1 = \zeta\rho_0$ (dashed lines), noting that no band gap is present.

4.1. Equivalent phononic response

It has already been noted that if the annular regions are chosen to be neo-Hookean with material properties related to the host via $\mu_1 = \zeta\mu_0$ and $\rho_1 = \zeta\rho_0$, the scattering properties of the deformed medium with deformed inner annular radii r_0 are equivalent to those of an undeformed medium with *uniform* properties μ_0 and ρ_0 and inner annular radii R_0; this property has been exploited in the study of elastodynamic cloaking for SH waves by choosing R_0 to be small and $r_0 \gg R_0$ [37]. These two materials are phononically equivalent, as illustrated in Fig. 2. Thus, the material could have quite distinct geometrical characteristics but its phononic behaviour would be equivalent. In particular, it is noted that this effect would permit a wide range of periodic materials, each medium having different cavity radii but identical phononic response.

This effect is exemplified in Fig. 3. The equivalence is illustrated in 3(a), taking a medium with $R_0 = 0.1$, the dispersion curves associated with the unstressed scenario where the host medium is uniform (having properties μ_0 and ρ_0) is plotted as solid lines and the pre-stressed neo-Hookean case (with annular properties $\mu_1 = \zeta\mu_0$ and $\rho_1 = \zeta\rho_0$) is indicated with circles. The Mooney–Rivlin case with $S_1 = 0.6$ is also shown to illustrate the effect that the strain energy function has on the invariance of the band structure. This reveals that we must be careful about the choice of constitutive material. In Fig. 3(b) a material with a band gap present (with $R_0 = 0.35$) is compared to an invariant material where no band gap is present, even though the deformed inner radius is also $r_0 = 0.35$.

4.2. A phononic cloak

Suppose that for some application it is required to have a medium with an array of regularly spaced cylindrical cavities of a specific radius large enough to cause band gaps. However one may wish to have such an inhomogeneous medium but
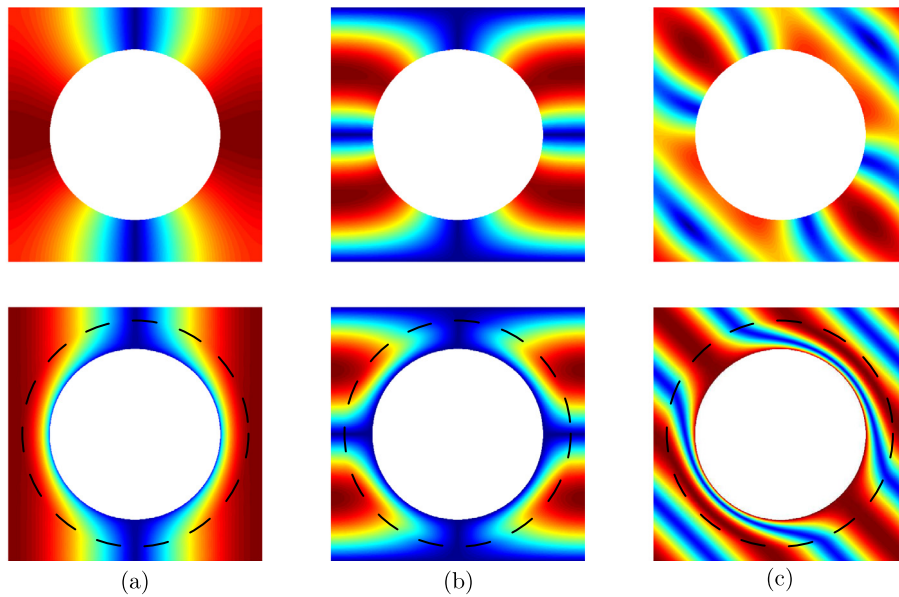
Fig. 4. Mode shapes for a periodic cell of a phononic cloak. The top row shows a stress-free homogeneous host material with cavities of radius $R_0 = 0.33$. The bottom row shows a pre-stressed material with $R_0 = 0$, $\zeta = 2.2$, $r_0 = 0.33$. Material properties in the annular region shown with the dashed line are chosen to be $\mu = \zeta\mu_0$ and $\rho = \zeta\rho_0$. In (a) and (b) $k_x = \pi$, $k_y = 0$, in (c) $k_x = \pi/2$, $k_y = \pi/2$.

not generate band gaps. A mechanism to achieve this is to use the invariance principle above. By choosing annular cylinders of small initial radii, we can make a material which geometrically, one would expect to experience band gaps, but due to the inhomogeneous properties it does not. If one were to choose initial radii that are small enough, the pre-stressed material with *large* radii would look almost identical to a homogeneous medium. One could term this material a *phononic cloak*.

In Fig. 4 we see three different mode shapes in the cell for a stress-free (top row) and pre-stressed (bottom row) material. In the pre-stressed case we have chosen a "perfect" cloak, with $R_0 = 0$. such that even in the deformed configuration the properties are identical to a homogeneous material. It is particularly evident in Fig. 4(c) that the wave interacts significantly with the cavity in the stress-free case, but refracts around the cavity in the pre-stressed material.

4.3. Effective behaviour and configurable band gaps

As demonstrated, the plane-wave-expansion method determines the wave structure of the medium with any choice of linear elastic shear moduli and densities of the annulus and host phases. However, henceforth for simplicity the properties of the host and annulus are set equal, i.e. $\mu_1 = \mu_0$ and $\rho_1 = \rho_0$. Before the effects of pre-stress on band gaps are considered in any detail an important aspect is studied—the influence of the pre-stress on the effective homogenised response at low frequency.

4.3.1. Effective behaviour at low frequency

The effective homogenised behaviour is obtained by determining the slope of the dispersion curves near the origin. This gives the phase velocity of the wave c_* and since it is known that at low frequency the effective density is given by $\rho_* = (1 - \phi)\rho_0$ (where ϕ is the volume fraction of cavities in the deformed configuration) the effective shear modulus is thus given by $\mu_* = \rho_* c_*^2$. Of specific interest here is how the pre-stress, and consequent localised deformation within the annulus region, modifies this effective response.

We can see in Fig. 5(a) how the wavespeed varies with inner radius. The solid line shows the stress-free case where we observe that the increase of the cavity radius causes the effective wavespeed to decrease. For the neo-Hookean (dashed) and Fung (dot-dash) models there is an increase in the effective wavespeed, whereas for the Mooney–Rivlin (dotted) model, with the parameter chosen to be $S_1 = 0.6$, there is almost no change in the effective wavespeed. The Fung strain energy function causes a significantly larger increase in the effective wavespeed over the entire range of radii, presumably due to the increased stiffness resulting from the exponential form of the strain energy function. This shows that the choice of strain energy function has a significant effect on the low frequency homogenised behaviour of the periodic solid. Note that neither neo-Hookean or Fung has an I_2 strain invariant dependence, which is therefore assumed to generate the rather different response of the Mooney–Rivlin medium [42].
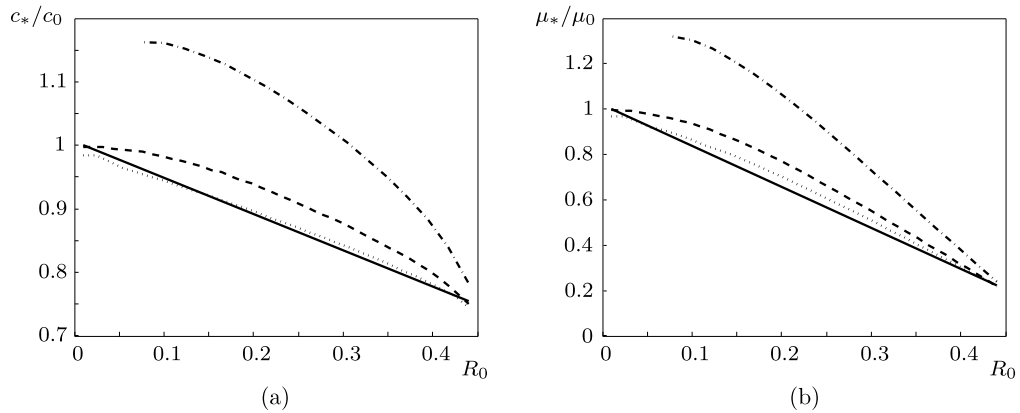
Fig. 5. The variation in (a) the effective wavespeed and (b) the effective shear modulus with undeformed cavity radius, scaled on the speed and shear modulus in the stress-free host, respectively. Solid lines show the stress-free case, dashed lines the neo-Hookean case, dotted lines the Mooney–Rivlin case ($S_1 = 0.6$) and the dot-dash lines the Fung case. In the pre-stressed materials an axial stretch of $\zeta = 1.2$ is applied.
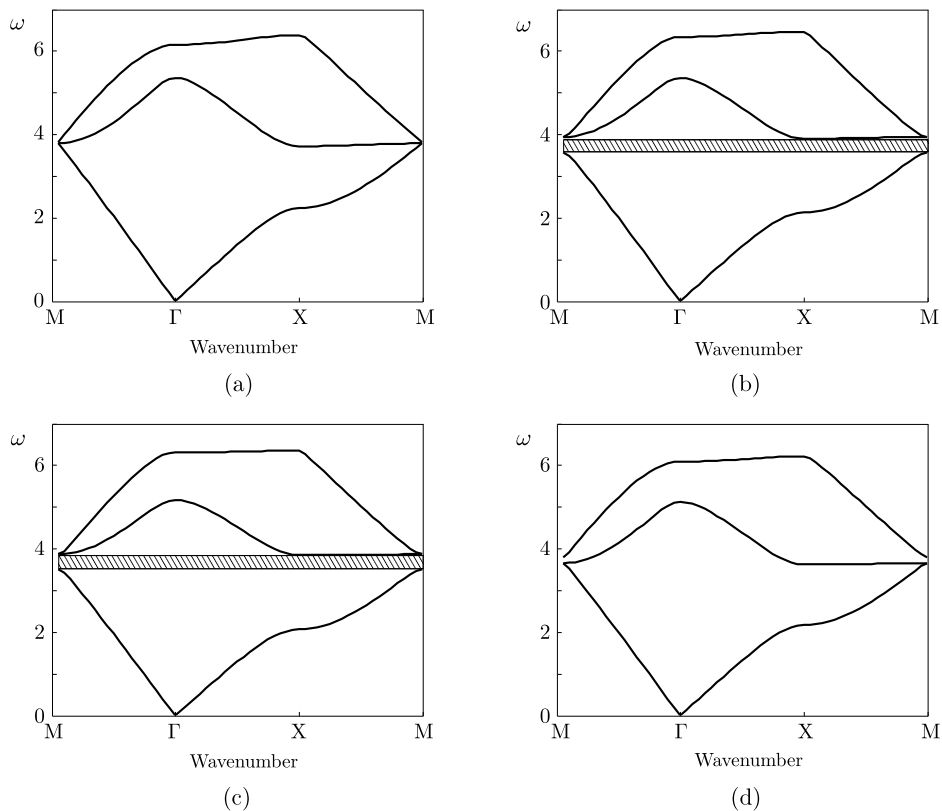

Fig. 6. The first three modes for a neo-Hookean cylinder. Stop bands are indicated by the shaded regions. Figure (a) shows the stress-free case with inner radius $R_0 = 0.3$; (b) the deformed configuration corresponding to initial inner radius $R_0 = 0.3$, an axial stretch $\zeta = 1.5$ and deformed inner radius $r_0 = 0.357$; a stop band has been "switched on". (c) The stress-free case with inner radius $R_0 = 0.35$; and (d) the deformed configuration corresponding to an initial inner radius $R_0 = 0.35$, an axial stretch $\zeta = 0.6$ and deformed inner radius $r_0 = 0.263$. The stop band has been "switched off" in this case.

4.3.2. Band gap tuning

We now investigate the effect of the pre-stress on the shape of the band gap with the idea of selectively activating or de-activating band gaps. Although it is possible to find interesting behaviour within the Brillouin zone [41] this behaviour is not of interest to us here since only stop bands are being sought. The band diagrams of the first three modes in a number of cases are plotted in Figs. 6 and 8. Fig. 7 shows the band gap widths for the alternative nonlinear materials considered here. These different materials are considered in turn and are then compared.
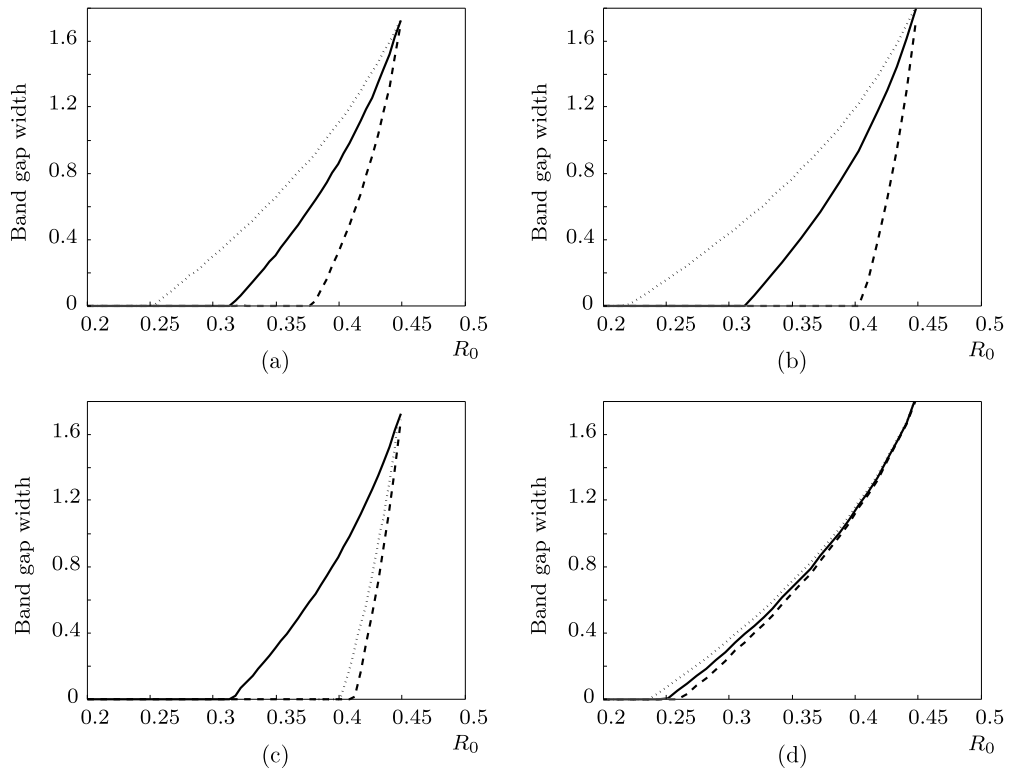
Fig. 7. The band gap width against undeformed inner radius, for various values of pre-stress in the cases of a (a) neo-Hookean medium, (b) the Mooney–Rivlin material with $S_1 = 0.6$, and (c) the Fung medium. Shown are axial stretches of $\zeta = 1$ (solid), $\zeta = 0.8$ (dash) and $\zeta = 1.2$ (dotted). In (d) we plot the band gap width of the Mooney–Rivlin strain energy function for a pre-stress of $\zeta = 1.4$ and various values of S_1 corresponding to $S_1 = 1$ (dashed), $S_1 = 0.8$ (solid) and $S_1 = 0.6$ (dotted).

Neo-Hookean material

Consider first the simplest strain energy function—the neo-Hookean material. Shown in Fig. 6(a) and (b) are the first three modes for the case when the annulus has an initial inner radius of $R_0 = 0.3$ in the stress-free configuration and the pre-stressed configuration corresponding to $\zeta = 1.5$ (for which the deformed inner radius is $r_0 = 0.357$) respectively. It is clearly seen by comparing (a) and (b) that a stop band has been switched on by this inflation. Additionally, it is noted that the dispersion curves associated with the wavenumber regions between Γ and X for the third mode have become flatter, indicating that the pre-stress has induced regimes of very slow waves.

In Fig. 6(c) and (d) the opposite effect is illustrated. A naturally occurring stop band in the *unstressed* material is switched off by lowering the internal pressure (or equivalently, applying an axial contraction) and decreasing the inner radius. In this case, the first three bands are plotted for an initial inner radius of the annulus of $R_0 = 0.35$ in the stress-free configuration alongside the first three bands for the pre-stressed configuration corresponding to $\zeta = 0.6$ (for which the deformed inner radius is $r_0 = 0.263$).

Fig. 7(a) shows how the width of the band gap varies with the undeformed inner radius. Illustrated are three different axial stretches, $\zeta = 0.8$ (deflation), $\zeta = 1.2$ (inflation) alongside the stress-free case $\zeta = 1$. In the stress-free case, a band gap opens up slightly above $R_0 = 0.3$ and then grows as R_0 increases. The same behaviour is experienced for the deformed configurations with larger band gaps for inflated cylinders. If one is to choose an initial radius below $R_0 = 0.31$, one could introduce a stop band by applying an appropriate amount of pre-stress.

Mooney–Rivlin material

Let us turn now to the effect of departure from neo-Hookean behaviour, by considering a Mooney–Rivlin material, reducing the parameter S_1 from unity, i.e. the neo-Hookean case. Fig. 8 illustrates the band structure resulting from an undeformed radius of $R_0 = 0.27$ alongside that of an inflated cylinder, with an axial stretch of $\zeta = 1.3$. In Fig. 8(b) the curves are plotted associated with the neo-Hookean case $S_1 = 1$, whereas in Fig. 8(c) we have a Mooney–Rivlin medium with $S_1 = 0.5$. It is seen that even with this rather large change to the constitutive behaviour (S_1 is normally closer to unity in practice) it causes very little change in the shape of the band structure when compared to the neo-Hookean case. However, it is noted that for the same deformation a stop band is switched on in the Mooney–Rivlin case which is not present for the neo-Hookean case.
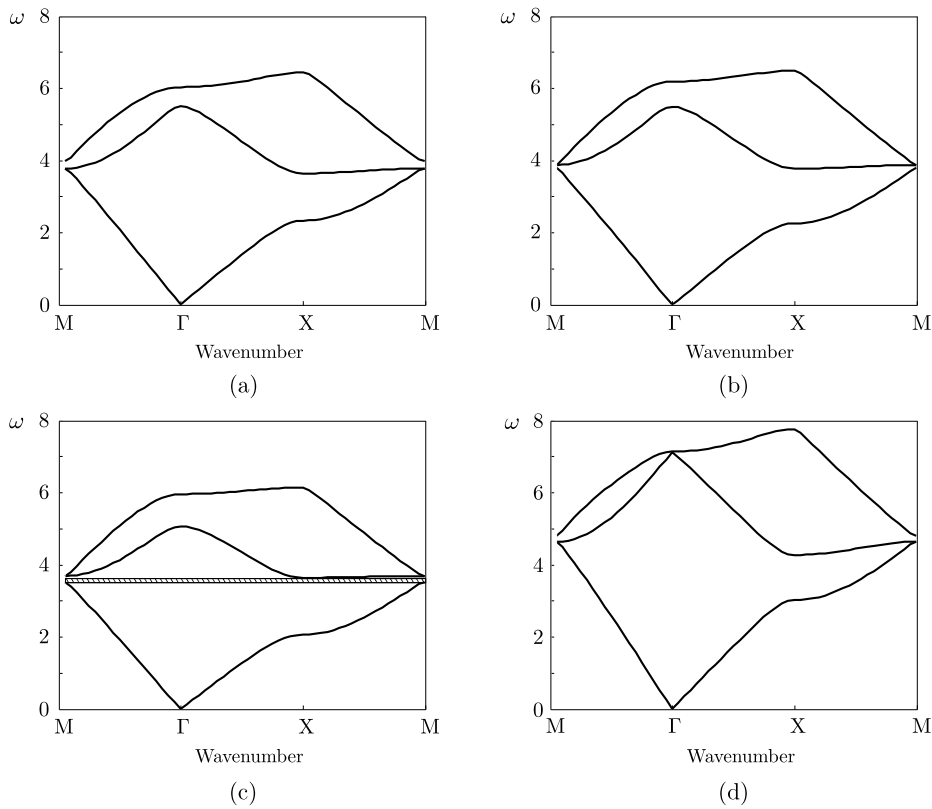
Fig. 8. The first three modes for a cylinder of initial radius $R_0 = 0.27$. Pictured are the band diagrams for (a) the stress-free case, alongside the deformed configuration with axial stretch $\zeta = 1.3$ and deformed inner radius $r_0 = 0.32$ for (b) a neo-Hookean material, (c) a Mooney–Rivlin material ($S_1 = 0.5$) and (d) a Fung-type material. Stop bands are shown by the shaded regions.

The band gap widths for the Mooney–Rivlin material are plotted in Fig. 7(b) for comparison with the neo-Hookean case. In agreement with the observation from the band diagrams, the choice of a Mooney–Rivlin material increases the widths of the band gaps. Aside from that, the widths follow very similar patterns. The presence of the strain invariant I_2 can be seen to widen band gaps in general. This is illustrated in Fig. 7(d), where the band gap width is depicted for a Mooney–Rivlin material for an axial stretch of $\zeta = 1.4$ and various values of S_1. The neo-Hookean case ($S_1 = 1$) is included for comparison. It is clear that decreasing the parameter S_1 increases the band gap width for all values of the undeformed radius. The difference is most noticeable for small radii. For initial radii above $R_0 = 0.3$ there is almost no difference between having a neo-Hookean or Mooney–Rivlin material.

Fung type material

In Fig. 8(d) the equivalent band diagram for a Fung material is plotted alongside the neo-Hookean and Mooney–Rivlin materials for an initial radius of $R_0 = 0.27$ and axial stretch $\zeta = 1.3$. Clearly using a Fung material has a significant effect on the lowest three modes, raising them to a higher frequency. This is likely due to the Fung material stiffening up significantly when large deformations are applied.

It is interesting to note that the stop band is not present for the Fung material, due to the significant change in the band gap shape. In particular, the frequency of the second band at point X is lower (in relation to the frequency at point M) when compared with the stress-free case. This appears to stop the band gap opening up.

Fig. 7(c) gives the band gap width for the Fung material as a function of undeformed radius. What is most interesting is that, contrary to the other materials, inflating a cavity in a Fung material always has the effect of decreasing the width of a stop band. This appears to happen for any amount of stretch. This highlights the point that the constitutive behaviour of the chosen material is extremely important. The Fung medium can in fact be seen as an extreme case of an 'I_1 only model'.

Influence of the choice of strain energy function

The difference between the strain energy functions considered here can be understood by analysing the inhomogeneous shear moduli. An increase in the S_1 towards unity (i.e. approaching the neo-Hookean case) accentuates the effect that the pre-stress has on the shear moduli. The neo-Hookean case is clearly the limit (in the context of the class of Mooney–Rivlin materials) at which there is maximum effect on the shear moduli, explaining why the effective wavespeed is so much higher in the neo-Hookean material. Due to the exponential nature of the Fung strain–energy function, the pre-stress has a much
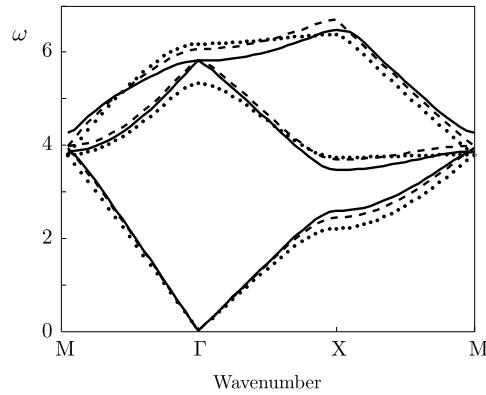
Fig. 9. The first three bands in the stress-free configuration with inner radius $R_0 = 0.2$ (solid line), the stress-free configuration with inner radius $R_0 = 0.3$ (dotted line) and the pre-stressed configuration with initial inner radius $R_0 = 0.2$, axial stretch $\zeta = 1.5$ and deformed inner radius $R_0 = 0.3$ (dashed line). This plot reveals that the pre-stress has an effect which goes further than just a change in geometry.

more significant effect on the shear moduli in comparison with the Mooney–Rivlin case. This leads to a more pronounced change in the band diagram as seen in Fig. 8(d). This behaviour can be associated with the I_1 only dependence and the Fung model is clearly an extreme example of such a model, given its exponential form.

4.4. Further observations

Further to the opening of stop bands, other more general observations can be made about the band diagrams. It is interesting to note that in both Figs. 3(a) and 8(d) the second and third bands are touching at the wavenumber Γ. In the Fung case, these intersecting bands are separated by a significant distance before the application of the pre-stress.

A final and important observation to be made is that the effect of the pre-stress goes further than just a change in the geometry. This can be seen from Fig. 9 in which the band diagram is plotted for a stress-free material alongside a pre-stressed medium, where the inner radius of the former is equal to the deformed inner radius of the latter. Although the shape of the bands are similar in some regions, there are several significant differences. For example, the difference in frequency at the wavenumber Γ is large when comparing the pre-stressed and equivalent material. This disparity implies that the inhomogeneity in the shear moduli caused by the deformation has a significant effect on the band structure.

5. Conclusion

A new geometrical design has been proposed in order to tune the band gap structure of a periodic elastic composite using nonlinear elastic pre-stress, thus permitting the design of phononic switches for antiplane elastic waves. In particular, the onset radius of the acoustic (lowest frequency) stop band has been investigated. It is found that applying an inflation inside the annulus tends to cause the stop band to switch on whereas a deflation tends to switch the band gap off. It was shown that the choice of material (via a variation of the strain energy function) has a significant influence on the size of the stop band. The concepts of phononic invariance and phononic cloaking were also introduced, in principal enabling a range of designs of materials with specific geometries and tunable band structures.

The approach utilised here is easily extendable to other configurations and more complex geometries, and indeed it is expected that this will provide a rich variety of band gap tuning strategies. In determining the band gap structure the plane-wave-expansion method was modified and extended in order to deal with material coefficients that are generally inhomogeneous, not simply piecewise constant as is almost always the case in standard problems. This extension will apply analogously to the coupled two- and three-dimensional elastodynamic problems, albeit with an obvious increase in complexity and system size.

Since the plane-wave-expansion method is implemented numerically, there are no restrictions on the geometries considered except for a limit on the size of the outer radius of the deformed cylinder; if the latter is too large then the cylinders get close to touching. In this case a large number of plane waves are required for convergence and although solvable, the computation becomes prohibitively slow on a standard desktop computer.

The only technical constraint of the present approach is our ability to find the incremental wave equation. Work is currently under way to investigate compressible hyperelastic materials, in which case an analytical solution for the nonlinear deformation is generally not possible; hence, a nonlinear ordinary differential equation must be solved numerically in order to determine the deformation. This will then necessitate a numerical approach to finding the incremental inhomogeneous moduli appearing in the incremental wave equation. For more complex geometries and loadings a numerical approach will also be required to determine the static deformation, associated stress fields, and incremental moduli.

Acknowledgements

References

[1] R. Craster, S. Guenneau, Acoustic Metamaterials: Negative Refraction, Imaging, Lensing and Cloaking, Springer, 2013.
[2] P. Deymier, Acoustic Metamaterials and Phononic Crystals, Springer, 2013.
[3] M. Sigalas, E.N. Economou, Elastic and acoustic wave band structure, J. Sound Vib. 158 (2) (1992) 377–382.
[4] M. Sigalas, E.N. Economou, Band structure of elastic waves in two dimensional systems, Solid State Commun. 86 (30) (1993) 141–143.
[5] M.S. Kushwaha, P. Halevi, L. Dobrzynski, B. Djafari-Rouhani, Acoustic band structure of periodic elastic composites, Phys. Rev. Lett. 71 (13) (1993) 2022–2025.
[6] M.S. Kushwaha, P. Halevi, G. Martinez, Theory of acoustic band structure of periodic elastic composites, Phys. Rev. B: Condens. Matter Mater. Phys. 49 (4) (1994) 2313–2322.
[7] M.I. Hussein, M.J. Leamy, M. Ruzzene, Dynamics of phononic materials and structures: Historial origins, recent progress and future outlook, Appl. Mech. Rev. 66 (2014) 040802.
[8] C. Goffaux, J.P. Vigneron, Theoretical study of a tunable phononic band gap system, Phys. Rev. B: Condens. Matter Mater. Phys. 64 (7) (2001) 5118–5122.
[9] X. Li, F. Wu, H. Hu, S. Zhong, Y. Liu, Large acoustic band gaps created by rotating square rods in two-dimensional periodic composites, J. Phys. D: Appl. Phys. 36 (1) (2003) 15–17.
[10] S.C.S. Lin, T.J. Huang, Tunable phononic crystals with anisotropic inclusions, Phys. Rev. B: Condens. Matter Mater. Phys. 83 (17) (2011) 4303–4312.
[11] A. Khelif, Two-dimensional phononic crystal with tunable narrow pass band: Application to a waveguide with selective frequency, J. Appl. Phys. 94 (3) (2003) 1308–1311.
[12] Y. Pennec, B. Djafari-Rouhani, J.O. Vasseur, A. Khelif, P.A. Deymier, Tunable filtering and demultiplexing in phononic crystals with hollow cylinders, Phys. Rev. E (3) 69 (4) (2004) 6608–6613.
[13] A. Evgrafov, C.J. Rupp, M.L. Dunn, K. Maute, Optimal synthesis of tunable elastic wave-guides, Comput. Methods Appl. Mech. Engrg. 198 (2) (2008) 292–301.
[14] X. Zhang, Z.-Q. Zhang, L.-M. Li, C. Jin, D. Zhang, B. Man, B. Cheng, Enlarging a photonic band gap by using insertion, Phys. Rev. B: Condens. Matter. Phys. 61 (3) (2000) 1892.
[15] O.B. Matar, J.F. Robillard, J.O. Vasseur, A.C. Hladky-Hennion, P.A. Deymier, P. Pernod, V. Preobrazhensky, Band gap tunability of magneto-elastic phononic crystal, J. Appl. Phys. 111 (5) (2012) 4901–4915.
[16] J.Y. Yeh, Control analysis of the tunable phononic crystal with electrorheological material, Physica B 400 (1) (2007) 137–144.
[17] W. Yang, L. Chen, The tunable acoustic band gaps of two-dimensional phononic crystals with a dielectric elastomer cylindrical actuator, Smart Mater. Struct. 17 (2008) 015011.
[18] Z. Hou, F. Wu, Y. Liu, Phononic crystals containing piezoelectric material, Solid State Commun. 130 (11) (2004) 745–749.
[19] X.Y. Zou, Q. Chen, B. Liang, J.C. Cheng, Control of the elastic wave bandgaps in two-dimensional piezoelectric periodic structures, Smart Mater. Struct. 17 (1) (2008) 5008–5012.
[20] F. Casadei, T. Delpero, A. Bergamini, P. Ermanni, M. Ruzzene, Piezoelectric resonator arrays for tunable acoustic waveguides and metamaterials, J. Appl. Phys. 112 (6) (2012) 4902–4906.
[21] X. Zhou, C. Chen, Tuning the locally resonant phononic band structures of two-dimensional periodic electroactive composites, Physica B 431 (1) (2013) 23–31.
[22] Z.G. Huang, T.T. Wu, Temperature effect on bandgaps of surface and bulk acoustic waves in two-dimensional phononic crystals, IEEE Trans. Ultrason. Ferroelectr. Freq. Control 52 (3) (2005) 365–370.
[23] K.L. Jim, C.W. Leung, S.T. Lau, S.H. Choy, H.L.W. Chan, Thermal tuning of phononic bandstructure in ferroelectric ceramic/epoxy phononic crystal, Appl. Phys. Lett. 94 (19) (2009) 3501–3503.
[24] J.Y. Ou, E. Plum, L. Jiang, N.I. Zheludev, Reconfigurable photonic metamaterials, Nano Lett. 11 (2011) 2142–2144.
[25] W. Zhu, Y. Huang, I.D. Rukhlenko, G. Wen, M. Premaratnel, Configurable metamaterial absorber with pseudo wideband spectrum, Opt. Express 20 (6) (2012) 6616–6621.
[26] G.A. Rogerson, K.J. Sandiford, The effect of finite primary deformations on harmonic waves in layered elastic media, Internat. J. Solids Structures 37 (14) (2000) 2059–2087.
[27] W.J. Parnell, Effective wave propagation in a pre-stressed nonlinear elastic composite bar, IMA J. Appl. Math. 72 (2) (2007) 223–244.
[28] G. Shmuel, G. deBotton, Band-gaps in electrostatically controlled dielectric laminates subjected to incremental shear motions, J. Mech. Phys. Solids 60 (11) (2012) 1970–1981.
[29] M. Gei, A.B. Movchan, D. Bigoni, Band-gap shift and defect induced annihilation in prestressed elastic structures, J. Appl. Phys. 105 (6) (2009) 3507–3513.
[30] R. Feng, K. Liu, Tuning the band-gap of phononic crystals with an initial stress, Physica B 407 (12) (2012) 2032–2036.
[31] L. Wang, K. Bertoldi, Mechanically tunable phononic band gaps in three-dimensional periodic elastomer structures, Internat. J. Solids Structures 49 (19) (2012) 2881–2885.
[32] K. Bertoldi, M.C. Boyce, Wave propagation and instabilities in monolithic and periodically structured elastomeric materials undergoing large deformations, Phys. Rev. B: Condens. Matter Mater. Phys. 78 (18) (2008) 4107–4122.
[33] J.H. Jang, C.Y. Koh, K. Bertoldi, M.C. Boyce, E.L. Thomas, Combining pattern instability and shape-memory hysteresis for phononic switching, Nano Lett. 9 (5) (2009) 2113–2119.
[34] R.W. Ogden, Non-linear Elastic Deformations, Dover, 1998.
[35] M. Destrade, G. Saccomandi, Waves in Nonlinear Pre-stressed Materials, Springer, New York, 2007.
[36] W.J. Parnell, Nonlinear pre-stress for cloaking from antiplane elastic waves, Proc. R. Soc. A: Math. Phys. Eng. Sci. 468 (2138) (2012) 563–580.
[37] W.J. Parnell, A. Norris, T. Shearer, Employing pre-stress to generate finite cloaks for antiplane elastic waves, Appl. Phys. Lett. 100 (17) (2012) 171907.
[38] W.J. Parnell, I.D. Abrahams, Antiplane wave scattering from a cylindrical void in a pre-stressed incompressible neo-Hookean material, Commun. Comput. Phys. 11 (2) (2012) 367–382.
[39] T. Shearer, Waves in nonlinear elastic media with inhomogeneous pre-stress (Ph.D. thesis), University of Manchester, 2012.
[40] Y.C. Fung, Biomechanics: Mechanical Properties of Living Tissues, Springer-Verlag, 1993.
[41] R. Craster, T. Antonakakis, M. Makwana, S. Guenneau, Dangers of using the edges of the Brillouin zone, Phys. Rev. B 86 (11) (2012) 5130–5135.
[42] C.O. Horgan, M.G. Smayda, The importance of the second strain invariant in the constitutive modeling of elastomers and soft biomaterials, Mech. Mater. 51 (2012) 43–52.